CHEMISTRY OF MATERIALS
ARTICLE
pubs.acs.org/cm

Thio- and Dithio-Biuret Precursors for Zinc Sulfide, Cadmium Sulfide, and Zinc Cadmium Sulfide Thin Films

Karthik Ramasamy, Mohammad A. Malik, Madeleine Helliwell, James Raftery, and Paul O'Brien*

The School of Chemistry and Manchester Materials Science Center, The University of Manchester, Oxford Road,
Manchester M13 9PL, United Kingdom

Supporting Information

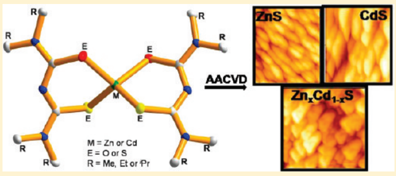

ABSTRACT: Zinc and cadmium complexes of 1,1,5,5-tetraalkyl-2-4-dithiobiurets $[M(N(SCNR_2)_2)_2]$ [M = Zn, R = methy (**1**), ethyl (**2**) and M = Cd, R = methyl (**4**), ethyl (**5**)] and 1,1,5,5-tetraalkyl-2-thiobiurets $[M(SON(CNR_2)_2)_2]$ [M = Zn, R = isopropyl (**3**) and M = Cd, R = isopropyl (**6**)] have been synthesized. The single crystal X-ray structures of complexes (**2**), (**3**), (**4**), and (**5**) were determined. Thermogravimetric analysis confirmed that all six complexes decomposed in a single step to their corresponding metal sulfides. The complexes were used as single source precursors for the deposition of zinc sulfide (ZnS), cadmium sulfide (CdS), and zinc cadmium sulfide ($Zn_xCd_{1-x}S$) thin films by aerosol assisted chemical vapor deposition (AACVD). The zinc complexes (**1**) and (**3**) deposited cubic ZnS films with small rods and granular crystallites at 300 and 350 °C, whereas at 400 and 450 °C hexagonal ZnS with granular crystallites were dominant. Complex (**2**) gave granular hexagonal ZnS films at all deposition temperatures. Cadmium complexes (**4**), (**5**), and (**6**) gave granular hexagonal CdS films at all deposition temperatures. $Zn_xCd_{1-x}S$ films were deposited by varying the relative concentration of precursors (**1**) and (**4**), (**2**) and (**5**), and (**3**) and (**6**) at 400 °C. The formation of a solid solution was confirmed by UV−vis spectroscopy and powder X-ray diffraction. The morphology of the films was studied by scanning electron microscopy and atomic force microscopy. The elemental composition of films was confirmed by energy dispersive X-ray spectroscopy.

KEYWORDS: single source precursors, zinc sulfide, cadmium sulfide, zinc cadmium sulfide, thin films

INTRODUCTION

Zinc sulfide has two main forms: cubic (sphalarite) and hexagonal (wurtzite). In addition to these, other polytypes are known.[1−4] These forms differ in the packing arrangement of the layers. Optical studies on the polytypes indicate that the absorption edge and birefringence can be correlated with the percentage of hexagonally stacked planes in the unit cell. The optical band gap of cubic ZnS, 3.5 eV, shifts to higher values with increasing pressure.[5] ZnS is used as a phosphor with Cu, Mn, and Ag added as activator or coactivator.[6,7]

CdS normally exists in hexagonal (greenockite) or cubic (hawleyite) forms,[8,9] and at high pressure, CdS transforms to an NaCl (halite) type structure.[10−12] Structural changes in CdS occur on electron irradiation.[13] CdS has interesting semiconducting and photoconducting properties. The mobility of charge carriers is strongly dependent upon temperature due to phonon scattering, in addition to polar acoustic modes at low temperature.[14] Measurements of the photo Hall effect indicate that Hall mobility increases with increasing carrier concentration by photon excitation.[15] In the wurtzite structure, CdS has a band gap of 2.58 eV, which increases with increasing pressure. The band structure of CdS is calculated to be similar to that of ZnS. The photo sensitivity of CdS can be altered by doping with impurities such as copper or iodide.[6]

ZnS or CdS thin films have been used for a wide variety of technological applications, including photovoltaic cells, electro-optic modulators, sensors, electroluminescent and photo luminescent devices, and antireflection coatings.[16−19] In particular, they have been widely employed in display technology as host lattices for doped phosphor materials, whose emission wavelength can be tailored as a function of the dopant metal.[17,20−22] The size and electronic structure of the cations added are sufficiently similar to Cd and/or Zn for the formation of solid solutions.[23] Thus, these are systems in which systematic variation of photoelectronic properties are possible simply by adjusting the composition.

In the wurtzitic structure, ZnS and CdS have unit cell volumes in the ratio of 0.77.[24] Because of such similarities, these materials have been widely employed in p−n junctions with a relatively small lattice mismatch in device based on quaternary materials like $CuIn_xGa_{1-x}Se_2$ or $CuIn(S_xSe_{1-x})_2$.[25,26] Thin films of $Zn_xCd_{1-x}S$ have properties between those of ZnS and CdS.[27−29] ZnS has a larger band gap than CdS, so all the $Zn_xCd_{1-x}S$ ternaries have larger energy bandgaps than CdS, which can make the materials attractive as windows in heterojunction photovoltaic devices such as CdS/CdTe solar cells.[30−35] Recently, Wang et al. detailed the use of ZnCdS in memory devices.[36]

The route used to prepare or deposit a material can profoundly affect the phase composition, thermal stability, and morphology, which in turn can influence the functional behavior

Received: October 22, 2010
Revised: December 23, 2010
Published: February 10, 2011

of the material. Many techniques have been used including sputtering,[37,38] pulsed laser ablation,[39,40] spray pyrolysis,[41,42] chemical bath deposition,[43,34] electrostatic-assisted aerosol jet deposition,[44,45] sol−gel,[46,47] ion-beam deposition,[48] and MOCVD.[49−57] MOCVD is well-known to give high-quality thin films. Various single source precursors have been investigated including metal complexes of dialkyldithiocarbamates,[51−54] alkyl xanthates,[49] and dimorpholino dithioacetylacetonates.[50] We have recently demonstrated that thio- and dithio-biuret metal complexes can be used as single source precursors for the preparation of various metal sulfide thin films[56−60] and nanoparticles.[61] In continuing this work, we report the synthesis of Zn and Cd complexes of 1,1,5,5-tetraalkyl-2-4-dithiobiurets (R = methyl or ethyl) and 1,1,5,5-tetraalkyl-2-thiobiurets (R = isopropyl) and their use as single molecular precursors for deposition of ZnS, CdS, and $Zn_xCd_{1-x}S$ thin films by AACVD.

EXPERIMENTAL SECTION

All preparations were performed under an inert atmosphere of dry nitrogen using standard Schlenk techniques. All reagents were purchased from Sigma-Aldrich chemical company and used as received. Solvents were distilled prior to use. ^1H and ^{13}C NMR studies were carried out using a Bruker AC300 FTNMR instrument. Mass spectra were recorded on a Kratos concept 1S instrument. Elemental analysis was performed by the University of Manchester microanalytical laboratory. TGA measurements were carried out by a Seiko SSC/S200 model under a heating rate of 10 °C min^{-1} under nitrogen. Melting point was recorded on a Stuart melting point apparatus and uncorrected.

X-ray Crystallography. Single-crystal X-ray diffraction data for the compounds were collected using graphite monochromated Mo Kα radiation (λ = 0.71073 Å) on a Bruker APEX diffractometer. The structures were solved by direct methods and refined by full-matrix least-squares on F^2.[62] All non-H atoms were refined anisotropically. H atoms were included in calculated positions, assigned isotropic thermal parameters, and allowed to ride on their parent carbon atoms. All calculations were carried out using the SHELXTL package.[63]

Deposition of Films by AACVD. In a typical deposition, about 200 mg of precursor was dissolved in 20 mL of THF in a two-necked 100 mL round-bottomed flask with a gas inlet that allowed the carrier gas (argon) to pass into the solution to aid the transport of the aerosol. This flask was connected to the reactor tube by a piece of reinforced tubing. The argon flow rate was controlled by a Platon flow gauge. Seven glass substrates (approximately 2 cm × 2 cm) were placed inside the reactor tube, which is placed in a CARBOLITE furnace. The precursor solution in a round-bottomed flask was kept in a water bath above the piezoelectric modulator of a PIFCO ultrasonic humidifier (Model 1077). The aerosol droplets of the precursor thus generated were transferred into the hot wall zone of the reactor by carrier gas. Both the solvent and precursor were evaporated, and the precursor vapor reached the heated substrate surface where thermally induced reactions and film deposition took place. For ternary films, different molar ratios of zinc and cadmium precursors were dissolved in 20 mL of THF. Deposition was carried out at 400 °C for 90 min.

Characterization of Thin Films. UV−vis spectra were measured using a Helios-Beta thermospectronic spectrophotometer. Measurements were made with a plain quartz substrate in the reference beam. Standardization was done by first replacing the coated substrate with a plain substrate in the sample position. X-ray diffraction studies were performed on a Bruker AXS D8 diffractometer using Cu Kα radiation. The samples were mounted flat and scanned between 20° to 80° in a step size of 0.05 with a count rate of 9 s. Films were carbon coated using Edward's E306A coating system before carrying out scanning electron microscopy (SEM) and energy dispersive X-ray spectroscopy (EDX) analyses. SEM analysis was performed using a Philips XL 30FEG, and EDX was carried out using a DX4 instrument. Atomic force microscopy (AFM) analysis was carried using Veeco CP2 instrument

*Synthesis of Bis(1,1,5,5-tetramethyl-2,4-dithiobiureto)zinc(II) [Zn(N(SCNMe$_2$)$_2$)$_2$] (**1**).* Dimethyl thiocarbamoylchloride (1.23 g, 10 mmol) and sodium thiocyante (0.813 g, 10 mmol) were added to 40 mL of acetonitrile, heated to reflux temperature, maintained for 1 h, and cooled to 25−30 °C. Filtered NaCl formed as side product. To the filtrate, 1.49 mL (20 mmol) of 60% solution of dimethylamine was added and stirred for 30 min at room temperature. Zinc acetate dihydrate (1.10 g, 5 mmol) was then added, stirring continued for 30 min. The product was isolated by filtration. Recrystallization was performed using a mixture of chloroform and methanol. Yield: 1.44 g (65%). Mp: 210 °C. ^1H NMR (300 MHz, $CDCl_3$, Me_4Si): 3.40 (s, 12 H), 3.15 (s, 12H), 4.38 (s, 2H). Elemental analysis. Calc for [$C_{12}H_{24}N_6S_4Zn$]: C, 32.3; H, 5.4; N, 18.8; S, 28.7; Zn, 13.8. Found: C, 32.1; H, 5.7; N, 18.7; S, 28.3; Zn, 14.6.

*Synthesis of Bis(1,1,5,5-tetraethyl-2,4-dithiobiureto)zinc(II) [Zn(N(SCNEt$_2$)$_2$)$_2$] (**2**).* Complex (**2**) was synthesized by the method described for complex (**1**) using diethylthiocarbamoyl chloride (1.51 g, 10 mmol) and diethylamine (1.91 mL, 20 mmol). The crude product was obtained as a white powder. Recrystallization from chloroform and methanol yielded colorless block crystals suitable for X-ray crystallography. Yield: 1.5 g, (54%). Mp: 120 °C. ^1H NMR (300 MHz, $CDCl_3$, Me_4Si): 3.4 (q, 8H), 3.8 (q, 8H), 1.0 (t, 12H), 1.1 (t, 12H). Elemental analysis. Calc. for $C_{20}H_{40}N_6S_4Zn$: C, 42.9; H, 7.1; N, 15.0; S, 22.9; Zn, 11.6. Found: C, 42.8; H, 7.3; N, 14.9; S, 22.6; Zn, 11.5.

*Synthesis of Bis(1,1,5,5-tetra-iso-propyl-2-thiobiureto)zinc(II) [Zn(SON(CN^{i}Pr$_2$)$_2$)$_2$] (**3**).* Complex (**3**) was synthesized by the method described for complex (**1**) using di-*iso*-propylcarbamoyl chloride (1.0 g, 6 mmol) and di-*iso*-propylamine (1.26 mL, 12 mmol). The crude product was isolated as a white powder. Recrystallization from chloroform and methanol yielded colorless needle crystals suitable for X-ray crystallography. Yield: 1.30 g, (67%). Mp: 298 °C. ^1H NMR (300 MHz, $CDCl_3$, Me_4Si): 4.75 (m, 4H), 3.5 (m, 4H) 1.1 (d, 24H), 1.4 (d, 24H). Elemental analysis. Calc. for $C_{28}H_{56}N_6S_2O_2Zn$: C, 52.7; H, 8.7; N, 13.1; S, 10.0; Zn, 10.2. Found: C, 52.2; H, 8.3; N, 12.7; S, 9.6; Zn, 9.8.

*Synthesis of Bis(1,1,5,5-tetramethyl-2,4-dithiobiureto)cadmium(II) [Cd(N(SCNMe$_2$)$_2$)$_2$] (**4**).* Complex (**4**) was synthesized by the method described for complex (**1**) using cadmium acetate dihydrate (1.33 g, 5 mmol) and was obtained as a white powder. Recrystallization from chloroform and methanol yielded colorless needles suitable for single crystal X-ray crystallography. Yield: 1.60 g, (65%). Mp: 90 °C. ^1H NMR (300 MHz, $CDCl_3$, Me_4Si): 3.4 (s, 12 H), 3.15 (s, 12H). Elemental analysis: Calc. for $C_{12}H_{24}N_6S_4Cd$: C, 29.2; H, 4.8; N, 17.0; S, 25.9; Cd, 22.8. Found: C, 28.8; H, 4.9; N, 16.7; S, 25.5; Cd, 22.7.

*Synthesis of Bis(1,1,5,5-tetraethyl-2,4-dithiobiureto)cadmium(II) [Cd(N(SCNEt$_2$)$_2$)$_2$] (**5**).* Complex (**5**) was synthesized by the method described for complex (**1**) using diethylthiocarbamoyl chloride (1.51 g, 10 mmol), diethylamine (1.91 mL, 20 mmol), and cadmium acetate dihydrate (1.33 g, 5 mmol). The crude product was obtained as a white powder. Recrystallization from chloroform and methanol yielded colorless block crystals suitable for X-ray crystallography. Yield: 1.6 g, (52%). Mp: 118 °C. ^1H NMR (300 MHz, $CDCl_3$, Me_4Si): 3.45 (q, 8H), 3.9 (q, 8H) 1.1 (t, 12H), 1.3 (t, 12H) Elemental analysis. Calc. for $C_{20}H_{40}N_6S_4Cd$: C, 39.6; H, 6.6; N, 13.8; S, 21.1; Cd, 18.5. Found: C, 39.5; H, 6.8; N, 13.8; S, 20.5; Cd, 18.1.

*Synthesis of Bis(1,1,5,5-tetra-iso-propyl-2-thiobiureto)cadmium(II) [Cd(SON(CN^{i}Pr$_2$)$_2$)$_2$] (**6**).* Complex (**6**) was synthesized by the method described for complex (**1**) using di-*iso*-propylcarbamoyl chloride (1.0 g, 6 mmol), di-*iso*-propylamine (1.26 mL, 12 mmol), and cadmium acetate dihydrate (0.81 g, 3 mmol). The crude product was isolated as a white powder. Yield: 1.49 g, (72%). Mp: 109 °C. ^1H NMR (300 MHz, $CDCl_3$,

Scheme 1. Schematic Representation of Synthesis of Ligand and Complexes

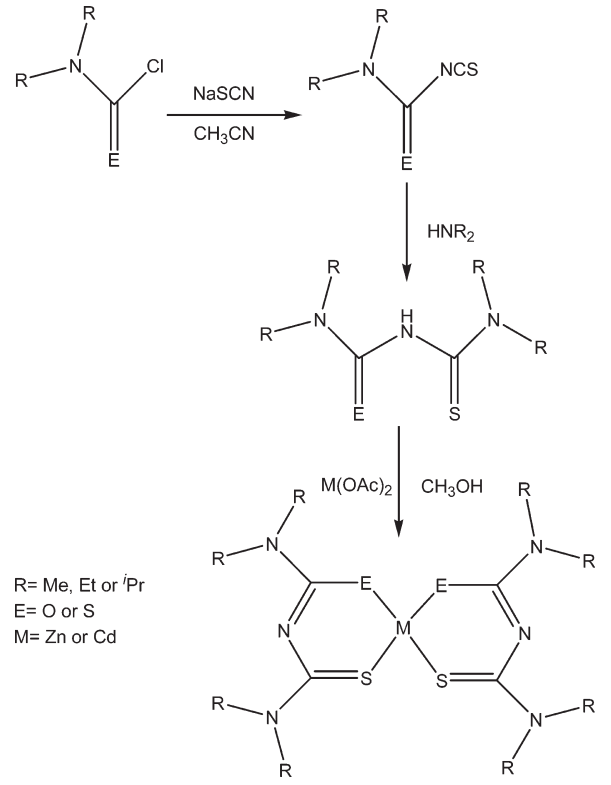

Me_4Si): 4.45 (m, 4H), 3.5 (m, 4H) 1.1 (d, 24H), 1.4 (d, 24H). Elemental analysis. Calc. for $C_{28}H_{56}N_6S_2O_2Cd$: C, 49.0; H, 8.1; N, 12.2; S, 9.3; Cd, 16.4. Found: C, 49.2; H, 7.8; N, 12.0; S, 9.1; Cd, 15.9.

■ RESULTS AND DISCUSSION

The zinc and cadmium complexes of thio- and dithio-biuret were synthesized by the reaction of excess dialkylamine with in situ generated dialkyl carbamoylthiocyanate in acetonitrile. The schematic representation of the synthesis of the complexes is shown in Scheme 1. All the complexes are air and moisture stable. Complexes (**1**), (**2**), (**4**), and (**5**) are soluble in toluene, tetrahydrofuran, chloroform, and other organic solvents. Complexes (**3**) and (**6**) are soluble in toluene, chloroform, and sparingly soluble in tetrahydrofuran.

Single Crystal X-ray Structure of [Zn(N(SCNEt$_2$)$_2$)$_2$] (2). The single crystal X-ray structure of complex (**2**) confirmed the formation of the expected bis-chelate complex as shown in panel (a) of Figure 1. The zinc atom has a distorted tetrahedral geometry with ligand bite angles of 102.55(2)° and 103.41(2)° that are smaller than the regular tetrahedral angle but slightly larger than those of the methyl analogue.[64] The ligand planes Zn(1)S(1)S(2) and Zn(1)S(3)S(4) are almost perpendicular, with an angle of 83.54(3)°. The distortion in geometry reflects in the zinc to sulfur bond distances, which vary from 2.3058(7) to 2.3174(7)Å and are similar to those in the methyl analogue.[64] In order to accommodate the Zn—S bonds and the wide bite angle, the two ligand frameworks in the crystal structure of complex (**2**) adopt torsional twists of 55.7(2)° and 56.0(2)° about the central N(2) and N(5) atoms, respectively, which are similar to those of the methyl derivative[64] but much larger than those of the methyl thiobiuret derivative.[64] The thiourea C—N bonds within the chelate ring are substantially shorter than the exocyclic C—NEt$_2$ bonds, indicating delocalization of the electrons in the six-membered (NC_2S_2—Zn) ring. Selected bond angles and bond lengths are given in the caption to Figure 1a.

Single Crystal X-ray Structure of [Zn(SON(CN^{i}Pr$_2$)$_2$)$_2$] (3). The single crystal X-ray structure of [Zn(SON(CN^{i}Pr$_2$)$_2$)$_2$] (**3**) illustrated in panel (b) of Figure 1 shows zinc in a distorted tetrahedral geometry with a S_2O_2 donor set. The two sulfur and two oxygen atoms are at the vertices of a tetrahedron. Both of the thiobiuret ligands of each unit are chelated to form two six-membered rings (NC_2OS—Zn). The ligand bite angles of 94.93(7) and 97.28(7) are smaller than the regular tetrahedral angle and slightly smaller than those observed for the methyl analogue.[64] This observation demonstrates a difference between superficially very similar complexes with rather different unit cells. The crystal lattice shows the presence of independent monomeric units, which are separated by normal van der Waals distances. Both of the thiobiuret ligands are nonplanar due to twisting about the central N atom. The average N—C—O and N—C—S angles are 126.0(2)° and 123.8(2)°, respectively. In both ligands, the pattern of bond distances indicates that the formal negative charge is predominately localized on the S atom. The relatively long C—S and short C—O average bond lengths of 1.785(3) and 1.267(3) Å, respectively, are consistent with mostly single- and double-bond characters, respectively. This bond localization is also reflected in the average C—N bond distances to the central N atoms: 1.318(3) Å in the thiourea group and 1.363(3) Å in the urea group. The average urea C—N bond, 1.363(3) Å, within the chelate ring is similar to the average exocyclic C—N^{i}Pr$_2$ bond, 1.349(2) Å, whereas the average thiourea C—N bond length, 1.318(3) Å, in the coordinating ring is somewhat shorter. The average metal to sulfur bond of 2.2703(7) Å is longer than metal to oxygen bond of 1.971(1).

Single Crystal X-ray Structure of [Cd(N(SCNMe$_2$)$_2$)$_2$] (4). The single crystal X-ray structure of the cadmium complex (**4**) shows that cadmium has a distorted tetrahedral geometry with ligand bite angles of 99.04(2)° and 96.46(2)°, which are smaller than those reported for the zinc complex (**1**)[64] and a regular tetrahedral angle. The C—N bond lengths to the central N atoms are equal within experimental error, average value 1.316(2) Å, indicating delocalization of electrons about the six-membered NC_2S_2—Cd ring. This value is shorter than the average exocyclic C—NMe$_2$ bond length of 1.341(2) Å. The average Cd—S bond length of 2.5274(4) Å also clearly supports the involvement of cadmium in the electron delocalization, although it is longer than the average bond length observed for the zinc complex of 2.3104(3) Å. Otherwise, the single crystal X-ray structure of complex (**4**) is similar to the zinc complex (**1**).[64]

Single Crystal X-ray Structure of [Cd(N(SCNEt$_2$)$_2$)$_2$] (5). The single crystal X-ray structure of complex [Cd(N(SCNEt$_2$)$_2$)$_2$] in panel (d) of Figure 1 shows cadmium in a distorted tetrahedral geometry. The complex crystallizes in the triclinic crystal system in the P-1 space group with two independent molecules in the asymmetric unit. Complex (**5**) is a structural analogue of zinc complex (**2**) and with similar geometric parameters to the methyl analogue (**4**) described in the previous section. Selected bond angles and bond lengths are given in the caption to Figure 1d.

Thermogravimetric Analysis (TGA). Thermogravimetric analysis gives an idea about the decomposition and/or volatility of the complexes. The TGA of zinc complexes (**1**), (**2**), and (**3**) indicated single-step decomposition with rapid weight loss between 249 and 348 °C, 258 and 344 °C, and 160 and 310 °C. The solid residue

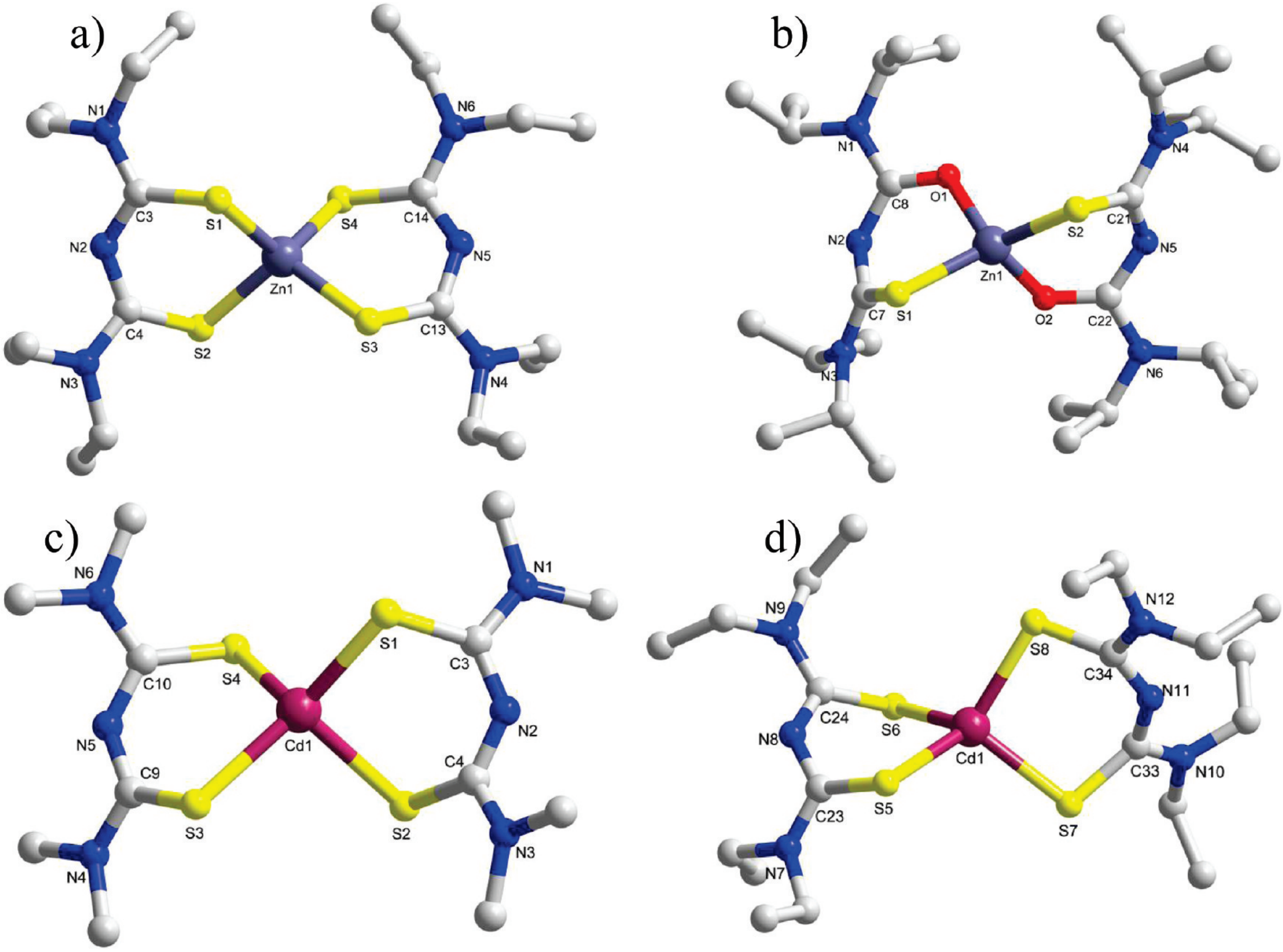

Figure 1. (a) X-ray structure of (**2**). Selected bond lengths (Å) and bond angles (deg): Zn1−S1 2.317(1), Zn1−S3 2.312(1), S1−C3 1.759(2), N1−C3 1.345(3) and S2−Zn1−S1 102.55(2), S3−Zn1−S4 103.41(2). (b) X-ray structure of (**3**). Selected bond lengths (Å) and bond angles (deg): Zn1−O1 1.972(2), Zn1−S1 2.269(1), S1−C7 1.789(4), O1−C8 1.254(4) and O1−Zn1−S1 94.93(7), O2−Zn1−S2 97.28(7). (c) X-ray structure of (**4**). Selected bond lengths (Å) and bond angles (deg): Cd1−S1 2.498(1), Cd1−S3 2.513(1), S1−C3 1.746(3), N1−C3 1.344(3) and S2−Cd1−S1 96.46(2), S3−Cd1−S4 99.04(2). (d) X-ray structure of (**5**). Selected bond lengths (Å) and bond angles (deg): Cd1−S5 2.516(1), Cd1−S7 2.499(1), S5−C23 1.752(2), N7−C27 1.464(2) and S6−Cd1−S5 98.24(2), S8−Cd1−S7 97.85(2).

amounts to 21.9% for (**1**), which is good agreement with the calculated value of 22.0% for ZnS. Similarly, the observed weights of the final residues are 16.6% for (**2**), and 14.1% for (**3**), which are close to calculated values of ZnS of 17.4% and 15.2%, respectively

The TGA of cadmium complexes (**4**), (**5**), and (**6**) showed single-step decomposition with weight loss between 258 and 388 °C, 247 and 344 °C, and 88 and 277 °C. The residue amounts to 33.0% for (**4**), which is close to calculated value of 30.0% for CdS, 20.1% for (**5**), and 19.2% for (**6**), which is also close to the calculated values for CdS of 23.8% and 21.0%, respectively

ZnS Thin Films. The apparatus used for the deposition of ZnS thin films is similar to that previously reported.[65] Glass substrates (2 cm × 2 cm, 7 or 8) were placed inside the reactor. Aerosols of thoroughly degassed solution of the precursor dissolved in THF (200 mg in 20 mL) were transported to the heated substrate using argon as a carrier gas at the flow rate of 160 sccm. ZnS thin films were deposited on glass substrates in the temperature range of 300−450 °C. Clean adhesive reflective uniform ZnS films were deposited at all temperatures from $[Zn(N(SCNMe_2)_2)_2]$ (**1**) and $[Zn(N(SCNEt_2)_2)_2]$ (**2**), whereas white, uniform, thick films were deposited from $[Zn(SON(CN^iPr_2)_2)_2]$ (**3**) at 300 and 350 °C, and dark uniform films were deposited at 400 and 450 °C.

Optical Band Gap. The optical band gap of the deposited ZnS films can be estimated from the UV spectra. The recorded spectra closely resembled those reported in the literature for ZnS.[66] As a general rule, ZnS coatings were completely transparent throughout the visible range, with a strong absorption at $\lambda \approx 380$ nm, ascribed to electronic interband transition from the filled sulfide (S 3p) valence band to empty conduction band, with a strong Zn(II) 4s character for ZnS. The optical band gap of the deposited films is influenced by two factors, the inherent band gap of the material and a tail due to disorder.[67] The energy band gap of the films were measured from the dependence of the absorption coefficient, α, on the photon energy, *hv*. In the present case, a plot of $(\alpha hv)^2$ versus *hv* is linear, indicating the direct band nature of the films. Extrapolating the linear portion of the curve onto the *X*-axis gives the band gap for the film. The evaluated band gaps are 3.23 eV (300 °C), 3.34 eV (350 °C), 3.35 eV (400 °C), and 3.36 eV (450 °C) for $[Zn(N(SCNMe_2)_2)_2]$ (**1**);

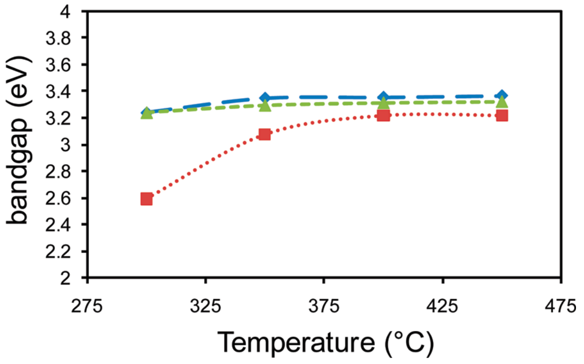

Figure 2. Graph showing variation of ZnS band gap versus deposition temperatures using (◆) [Zn(N(SCNMe$_2$)$_2$)$_2$] (**1**), (■) [Zn(N(SCNEt$_2$)$_2$)$_2$] (**2**), and (▲) [Zn(SON(CN^{i}Pr$_2$)$_2$)$_2$] (**3**).

2.62 eV (300 °C), 3.07 eV (350 °C), and 3.21 eV (400 and 450 °C) for [Zn(N(SCNEt$_2$)$_2$)$_2$] (**2**); and 3.23 eV (300 °C), 3.29 eV (350 °C), 3.30 eV (400 °C), and 3.31 eV (450 °C) for [Zn(SON(CN^{i}Pr$_2$)$_2$)$_2$] (**3**) (Supporting Information). The variation of energy band gap, E_g, as a function of deposition temperature is shown in Figure 2.

The band gap was found to increase with increasing deposition temperature. It is well-known that the energy band gap of a semiconductor is affected by the residual strain, defects, charged impurities, disorder at the grain boundaries, and also particle size confinement.[68] In addition, the tensile strain will result in a decrease in band gap due to the elongated lattice, whereas a compressional strain increases the band gap because of the the compressed lattice of the film.

Structural Studies. The powder X-ray diffraction (PXRD) patterns of zinc sulfide thin films deposited on glass substrate from precursor [Zn(SON(CN^{i}Pr$_2$)$_2$)$_2$] (**3**) are shown in Figure 3. The intense peak at 2θ 28.6° (d = 3.12 Å) corresponds to the hexagonal (002) (ICDD: 008-7254) and/or cubic (111) reflections of ZnS (ICDD: 003-0570). The very weak lines at 2θ 51.9° (d = 1.76 Å) and 2θ 59.3° (d = 1.56 Å) correspond to hexagonal (103) planes and hexagonal (004) and/or cubic (222) planes, respectively.

Precursor (**1**) at 350 °C gives the cubic phase, and above 400 °C the hexagonal phase is seen as confirmed by a second intense reflection at 2θ 47.8° (d = 1.91 Å). The reflection at the d = 1.76 Å (103) plane is unique to the hexagonal phase. A similar cubic to hexagonal phase transition above 400 °C is observed with precursor (**3**). In contrast to these results, only the hexagonal phase of zinc sulfide films was observed using precursor (**2**) (Figure 4).

Wold et al. reported that the temperature, sulfur fugacity, and nature and orientation of substrates are the three major parameters that decide the phase, cubic or hexagonal, of ZnS deposition.[4] In our system, the temperature or sulfiding nature of the precursors could be the reason for the deposition of cubic or hexagonal ZnS films. ZnS film depositions from precursors (**1**) and (**3**) were similar to Wold et al. observations. The various factors that influence the stable polycrystalline state of a material include the lowest surface energy, grain boundary energy, and diffusion of surface atoms.[69] The reports by Lee et al.[70] show that the strain energy minimization and surface energy minimization compete with one another to determine the preferred orientation of grain growth and the final texture of thin films. The minimization of strain energy promotes one type of texture, while the minimization of surface energy promotes another. In thinner films, surface energy dominates, whereas at greater thickness strain energy will be significant. The surface structure of the substrate forces the nuclei to grow along a specific orientation preventing nucleation along other orientations.[71] It can be concluded from the above discussion that the interaction at the film and substrate interface could be high at lower deposition temperatures. This could cause the film to grow in cubic structure. The influence of the substrate might be reduced with an increase in film thickness at higher deposition temperatures.

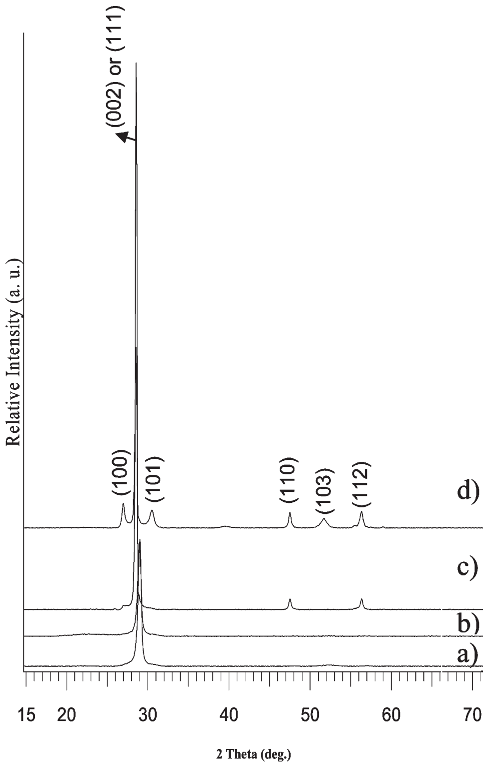

Figure 3. PXRD pattern of ZnS films deposited using [Zn(SON(CN^{i}Pr$_2$)$_2$)$_2$] (**3**) at (a) 300 °C, (b) 350 °C, (c) 400 °C, and (d) 450 °C on glass substrate.

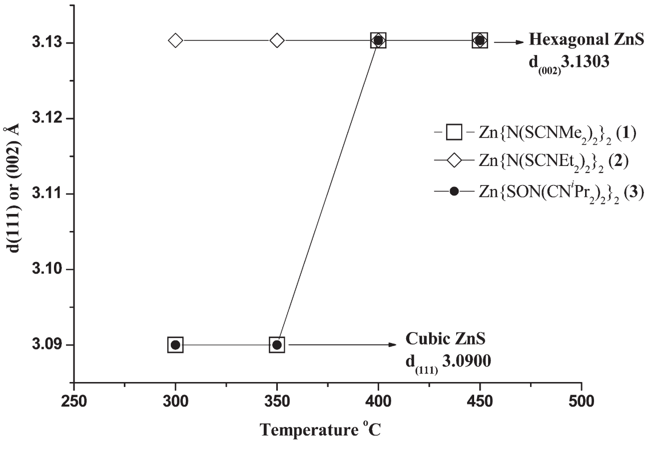

Figure 4. Graph showing change of cubic to hexagonal ZnS films deposited from complexes (**1**), (**2**), and (**3**) at temperatures between 300 and 450 °C.

Unequivocal characterization of the crystallographic phase is difficult for oriented ZnS films and is often absent in the

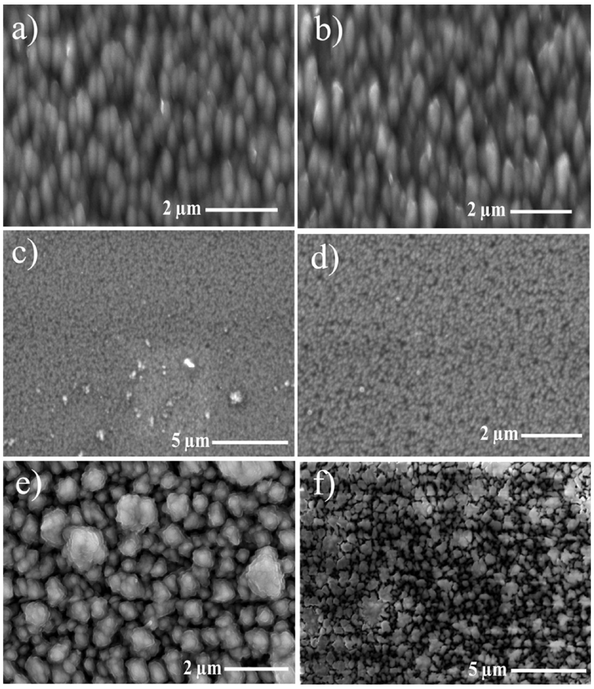

Figure 5. SEM image of ZnS films deposited using [$Zn(N(SCNMe_2)_2)_2$] (1) at (a) 400 °C and (b) 450 °C, [$Zn(N(SCNEt_2)_2)_2$] (2) at (c) 400 °C and (d) 450 °C, and [$Zn(SON(CN^iPr_2)_2)_2$] (3) (e) 400 °C and (f) 450 °C.

literature. The growth of hexagonal ZnS films generally occurs at higher temperatures but can also occur at temperatures as low as 300 °C.[4] The coexistence of a zinc-blende and wurtzite structure for ZnS has been reported in the literature.[4,72,73] Johnston et al.[74] and Cheng et al.[75] reported the hexagonal structure, while Saratale et al.[76] and Lee et al.[77] reported the cubic structure for the films prepared by chemical bath deposition. Elidrissi et al. reported that ZnS films grown by spray pyrolysis on glass substrates exhibited a mixture of both cubic and hexagonal phases.[78] This analysis shows that the presence of a crystalline phase in ZnS films is sensitive to the method of preparation, the substrates used to prepare the films, and the deposition temperature.[73] Generally, in polycrystalline thin film structures, the predominant structure or orientation mainly depends on the processing parameters. The structural changes occur by surface diffusion and migration of grain boundaries during the coalescence of two differently oriented nuclei. In such cases, smaller nuclei may more easily rotate on coalescence to induce the structural changes.[79]

Morphological Studies. The SEM images of ZnS thin films grown on glass substrate for 1.5 h at a temperature range of 300−450 °C, using precursors [$Zn(N(SCNMe_2)_2)_2$] (**1**), [$Zn(N(SCNEt_2)_2)_2$] (**2**), and [$Zn(SON(CN^iPr_2)_2)_2$] (**3**), are shown in Figure 5. Images show that dense and well-arranged approximately 1 µm long vertical rod-like crystallites were deposited from (**1**) at 450 °C, 800 ± 30 nm length rods at 400 °C, and irregular crystallites at 350 and 300 °C, with the size of 550 ± 25 nm and 400 ± 35 nm, respectively. Highly packed spherical crystallites were deposited from precursor (**2**) at all temperatures with the size range of 300 ± 20 to 450 ± 30 nm. In contrast to these morphologies of crystallites deposited from precursors (**1**) and (**2**), granular crystallites were deposited from precursor (**3**), with an approximate size range of 800 ± 35 to 1300 ± 50 nm at 300−450 °C. The increase in crystallites size with an improved crystallinity at higher temperature follows the results obtained by PXRD and UV spectra. EDX measurements with a power source of 20 kV for the films deposited on glass substrate show that the percentages of Zn:S composing the films are Zn:S 47:53 at 300 °C, 48:52 at 350 °C, and 50:50 at 400 °C, and 52:48 at 450 °C from precursor (**1**); Zn:S 48:52 at 300 °C, 50:50 at 350 and 400 °C, and at 51:49 at 450 °C from precursor (**2**); and Zn:S 48:52 at 300 and 350 °C, 50:50 at 400, and 51:49 at 450 °C from precursor (**3**).

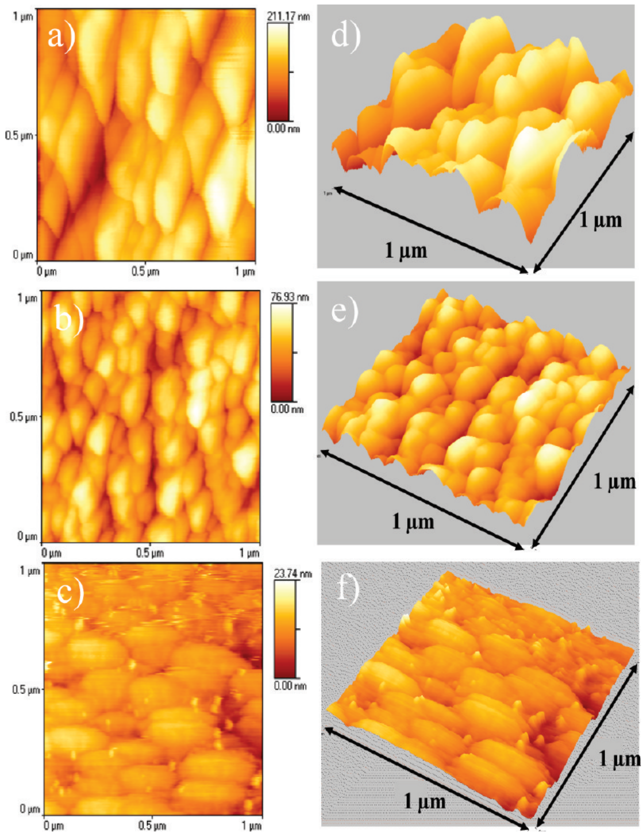

Figure 6. AFM images of ZnS films deposited at 400 °C (a). (d): 2-D and 3-D images of films from [$Zn(N(SCNMe_2)_2)_2$] (**1**). (b) and (e): 2-D and 3-D images of films from [$Zn(N(SCNEt_2)_2)_2$] (**2**). (c) and (f): 2-D and 3-D images of films from [$Zn(SON(CN^iPr_2)_2)_2$] (**3**).

The AFM measurements were performed to analyze the topography of the as-deposited films. Figure 6 shows the surface morphology of ZnS films prepared from three different precursors. These images show the presence of uniform and crack-free surface morphologies characterized by well-interconnected rods. The typical root-mean-square roughness was 25−30 nm at deposition temperatures from 300 to 450 °C. Films were deposited using precursor (**1**). Similarly well-connected closely packed crystallites were seen from the AFM images of films deposited from precursor (**2**) with the typical root-mean-square roughness of 22−28 nm at temperatures from 300 to 450 °C. AFM images of films deposited from precursor (**3**) show closely packed granular crystallites with the typical root-mean-square roughness of 34 to 40 nm at temperatures from 300 to 450 °C. The increase in surface roughness with increasing deposition temperature is associated with an increase in grain size. As the grain grew larger, the density of grain boundaries decreased, and the grain growth took place with a large variation in the height of the grain on the film surface. Therefore, it is apparent that the deposition temperature of the film changes the grain sizes as well as the surface roughness.

CdS Thin Films. The apparatus used for the deposition of CdS thin films is the same as for ZnS. Glass substrates (2 cm × 2 cm, 7 or 8) were placed inside the reactor. Aerosols of a thoroughly degassed solution of precursors (**4**), (**5**), or (**6**) dissolved in THF (200 mg in 20 mL) transported to the heated substrate using argon as a carrier gas at the flow rate of 160 sccm. CdS thin films were deposited on glass substrates at temperatures ranging from 350 to 500 °C. No deposition was observed below 350 °C and above 500 °C from all three precursors. Yellowish specular CdS films were deposited on glass substrates at 350 and 400 °C. Dark yellow films were deposited at 450 and 500 °C from $[Cd(N(SCNMe_2)_2)_2]$ (**4**). Reflective yellow films of CdS were deposited on glass substrates at 350 and 400 °C. Brownish films were deposited at 450 and 500 °C from $[Cd(N(SCNEt_2)_2)_2]$ (**5**), whereas uniform, thick, yellow films were deposited at 350−500 °C from $[Cd(SON(CN^iPr_2)_2)_2]$ (**6**).

Optical Band Gap. The optical band gap of the CdS films deposited from precursors (**4**), (**5**), and (**6**) were estimated from the UV spectra. The recorded band gaps are in good agreement with literature values.[43] The red shift in the fundamental absorption edge with increasing deposition temperature indicates the growth of larger crystallites at higher temperatures.

It is well known that the energy band gap of a semiconductor is affected by the residual strain, defects, charged impurities, disorder at the grain boundaries, and also particle size confinement. Increase in absorption intensity at higher deposition temperatures also confirms the deposition of thicker films. Cadmium sulfide has a strong absorption at $\lambda \approx 530$ nm, corresponding to the interband transition from the filled sulfide (S 3p) valence band to the empty conduction band, strongly Cd(II) 4s in character. The type of optical transition and energy band gap of the films were measured from the dependence of absorption coefficient (α) on the photon energy (hv).

In the present case, the linear plot of $(\alpha hv)^2$ versus hv indicates the direct band nature of the CdS films, and extrapolating the linear portion of the curve onto the *X*-axis gives the band gap for the film. The evaluated energy band gaps are 2.31 eV (350 °C), 2.39 eV (400 and 450 °C), and 2.43 eV (500 °C) for $[Cd(N(SCNMe_2)_2)_2]$ (**4**); 2.32 eV (350 °C), 2.38 eV (400 °C), 2.40 eV (450 °C), and 2.41 eV (500 °C) for $[Cd(N(SCNEt_2)_2)_2]$ (**5**), and 2.34 eV (350 °C), 2.38 eV (400 °C), 2.39 eV (450 °C), and 2.41 eV (500 °C) for $[Cd(SON(CN^iPr_2)_2)_2]$ (**6**). The variation of energy band gap, E_g, as a function of deposition temperature is shown in Figure 7. The band gap was found to increase with increasing deposition temperature. This observation may suggest the growth of larger crystallites at the higher deposition temperature.

Structural Studies. The powder X-ray pattern of cadmium sulfide thin films deposited on glass substrate from $[Cd(SON(CN^iPr_2)_2)_2]$ (**6**) is shown in Figure 8. PXRD patterns of CdS always show a well know complication of assigning the peaks to hexagonal or cubic polymorphs. Standard $\theta-2\theta$ scans cannot reliably distinguish (111)-oriented cubic CdS from hexagonal CdS (001) orientation.

However, in this study PXRD produced no evidence for cubic CdS in any films, and the following discussion assumes that they contain only the hexagonal phase formed under most film growth conditions.[80] The $\theta-2\theta$ XRD scans on films deposited on glass substrate showed the intense diffraction peaks at 24.7° (d = 3.59 Å), 26.4° (d = 3.36 Å), 28.1° (d = 3.17 Å), 43.8° (d = 2.08 Å), and 47.8° (d = 1.90 Å) from the films deposited at 350 and 400 °C using precursors (**4**) and (**5**). Whereas the only single intense peak at 26.6° (d = 3.38 Å) was observed from films deposited using precursor (**6**) at 350 and 400 °C, which indicates the preferred orientation along the (002) plane. The PXRD peaks from (**4**), (**5**), and (**6**) were indexed to (100), (002), (101), (110), and (103) planes of hexagonal CdS (ICDD: 01-075-1545). The lattice parameters (c) calculated from the largest diffraction plane (002) from the films deposited at 400 °C using precursors (**4**), (**5**), and (**6**) are 6.748, 6.763, and 6.758, respectively. The considerable increase in the c value from the bulk hexagonal CdS (c = 6.737) suggests the presence of a tensile strain along the c-axis.

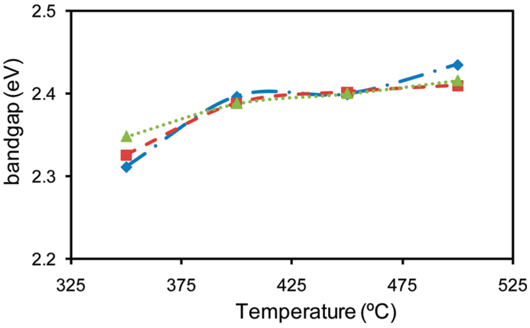

Figure 7. Graph showing variation of CdS band gap versus deposition temperatures using (♦) $[Cd(N(SCNMe_2)_2)_2]$ (**4**), (■) $[Cd(N(SCNEt_2)_2)_2]$ (**5**), and (▲) $[Cd(SON(CN^iPr_2)_2)_2]$ (**6**).

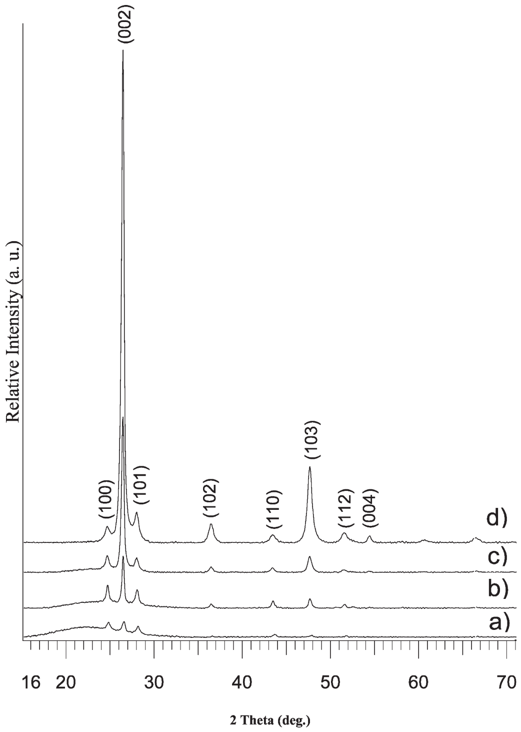

Figure 8. PXRD pattern of CdS films deposited using $[Cd(N(SCNEt_2)_2)_2]$ (**5**) at (a) 350 °C, (b) 400 °C, (c) 450 °C, and (d) 500 °C on glass substrate.

Morphological Studies. The SEM images of the films deposited from (**4**), (**5**), and (**6**) show growth of granular scattered

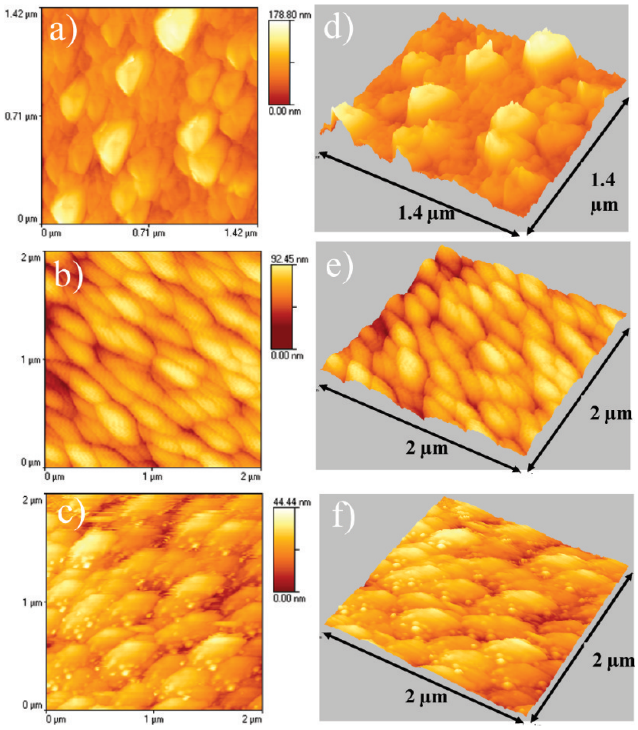

Figure 9. AFM images of CdS films deposited at 400 °C (a). (d): 2-D and 3-D images of films from $[Cd(N(SCNMe_2)_2)_2]$ (**4**). (b) and (e): 2-D and 3-D images of films from $[Cd(N(SCNEt_2)_2)_2]$ (**5**). (c) and (f): 2-D and 3-D images of films from $[Cd(SON(CN^iPr_2)_2)_2]$ (**6**).

crystallites over the entire glass substrate at 350 °C, whereas at 400 and 450 °C uniform larger crystallites were observed. The deposition from precursor (**4**) at 500 °C produced clusters of granular crystallites with an approximate size range from 200 ± 25 to 350 ± 30 nm. Spherical crystallites of 400 ± 35 to 550 ± 30 nm were observed from films deposited from using precursor (**5**) at deposition temperatures of 350 to 500 °C, whereas irregular granular cluster-like crystallites were deposited from precursor (**6**), with an approximate size range of 600 ± 50 to 1500 ± 30 nm. The composition of cadmium sulfide thin films deposited on glass substrates were analyzed by EDX measurement with a power source of 20 kV. The EDX analysis shows the percentage of Cd:S is 48:52 at 350 and 400 °C, 50:50 at 450 °C, and 52:48 at 500 °C for (**4**); Cd:S is 48:52 at 350 °C, 50:50 at 400 and 450 °C, and 51:49 at 500 °C for (**5**), and Cd:S is 47:53 at 350 and 400 °C, 50:50 at 450 °C, and 51:49 at 500 °C for (**6**).

The surface topography of the as-deposited films were analyzed by AFM. Figure 9 shows surface morphology of CdS films prepared from precursors (**4**), (**5**), and (**6**). AFM analysis from the films deposited using precursor (**4**) shows the presence of uniform and crack-free surface morphologies characterized by well-interconnected globular crystallites. The typical root-mean-square roughness was 20−27 nm at deposition temperatures of 350−500 °C. Similarly, well-connected closely packed crystallites were observed from the AFM images of films deposited from precursor (**5**) with the typical root-mean-square roughness of 11−15 nm at temperatures from 350 to 500 °C. AFM images of films deposited from precursor (**6**) show crack-free surfaces of granular crystallites with the typical root-mean-square roughness of 25−34 nm at temperatures from 350 to 500 °C. The increase in surface roughness with increasing deposition temperature is associated with an increase in grain size. It is apparent that the deposition temperature of the film changes the grain sizes as well as the surface roughness.

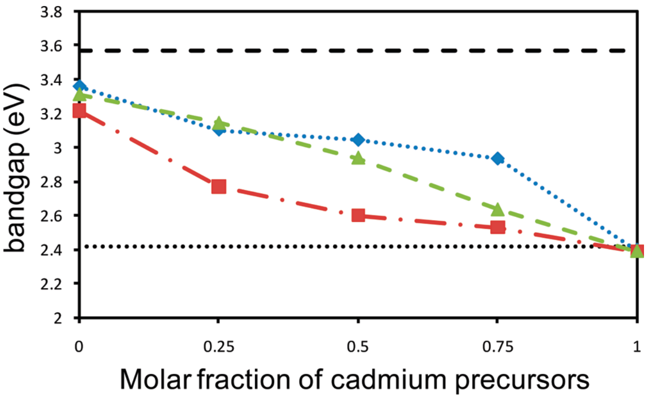

Figure 10. Optical band gap vs fraction of cadmium precursor (a) $Zn_xCd_{1-x}S$ films prepared using (♦) complexes (**1**) and (**4**), (■) complexes (**2**) and (**5**), and (▲) complexes (**3**) and (**6**). Dotted and dashed lines indicate the band gap of hexagonal CdS and ZnS.

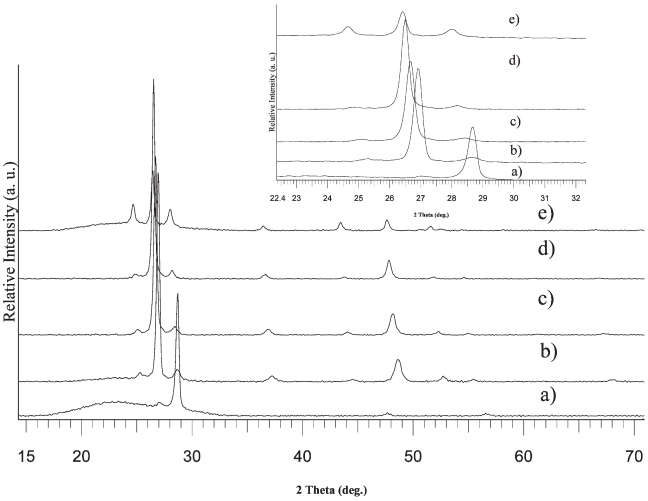

Figure 11. PXRD pattern of $Zn_xCd_{1-x}S$ films deposited using complex (**2**) and (**5**). Inset shows variation of (002) plane (a) ZnS, (b) ZnS at (0.25), (c) ZnS at (0.50), (d) ZnS at (0.75) molar fraction of cadmium precursor and (e) CdS films.

$Zn_xCd_{1-x}S$ Thin Films. Thermogravimetry confirmed that the zinc and cadmium precursors decompose to the corresponding metal sulfides at similar temperatures in a single step. This data suggests that the pairs of precursors fulfill the design requirement for deposition of $Zn_xCd_{1-x}S$ by AACVD. The deposition temperature for the formation of homogeneous $Zn_xCd_{1-x}S$ was identified from the individual experiments carried out with each precursor. Films were deposited at 400 °C by varying the ratio of precursors (**1**) and (**4**) in the delivery solution; x is the mole fraction of cadmium in this vessel throughout this section. The deposited films were colorless and uniform over the substrates at x = 0.25 of cadmium precursor (**4**). A slightly yellowish tinge was observed at x = 0.50, and yellowish reflective films were obtained at x = 0.75. Similar films were deposited using precursors (**2**) and (**5**), whereas films deposited using precursors (**3**) and (**6**) were

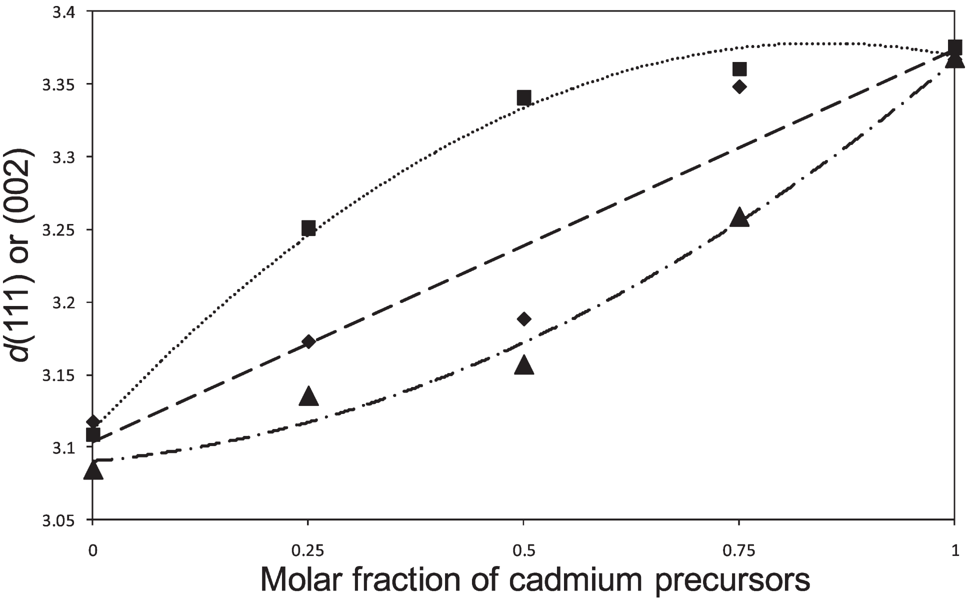

Figure 12. *d*(111) or (002) vs molar fraction of cadmium precursor (a) $Zn_xCd_{1-x}S$ films prepared using (♦) complexes (**1**) and (**4**), (■) $Zn_xCd_{1-x}S$ films prepared using complexes (**2**) and (**5**), and (▲) $Zn_xCd_{1-x}S$ films prepared using complexes (**3**) and (**6**).

thicker and uniformly colorless at x = 0.25 and 0.5 and yellowish reflective at x = 0.75.

Optical Band Gap. The optical spectra of the as-deposited films using precursors (**1**) and (**4**) were characterized by UV—visible spectroscopy. The value of the optical band gap (E_g) is estimated by plotting $(\alpha h\nu)^2$ versus $h\nu$, and $h\nu$ is the photon energy. Extrapolation of the linear portion of curve to $(\alpha h\nu)^2 = 0$ gives the optical band gap. The optical band gap of ZnS films deposited at 400 °C using precursor (**1**) is 3.35 eV and is 2.39 eV for the corresponding cadmium sulfide deposition from (**4**). The intermediate band gaps are 3.10 eV, x = 0.25; 3.04 eV, x = 0.50; and 2.93 eV, x = 0.75. The band gaps measured for precursors (**2**) and (**5**) are 2.76 eV, x = 0.25; 2.60 eV, x = 0.50; and 2.52 eV, x = 0.75. Similarly, the band gaps of films deposited from varying the ratio of precursors (**3**) and (**6**) are 3.14 eV, x = 0.25; 2.93 eV, x = 0.50; and 2.63 eV, x = 0.75. The red shift in optical absorption band edge of films shows formation of a solid solution. Figure 10 shows the band gap verses molar fraction of precursors in the delivery system. The variation in band gap is linear for precursor pair (**3**) and (**6**), which may indicate that these are the best matched of the three systems studied. The other pairs of precursors show positive or negative deviations from simple Vergard type behavior.

Structural Studies. The as-deposited $Zn_xCd_{1-x}S$ films were characterized by powder XRD. The X-ray diffractions confirm that all films are hexagonal. In assessing these results, we need to remember that at 400 °C all of the zinc precursors give predominantly hexagonal ZnS. Figure 11 shows XRD patterns of $Zn_xCd_{1-x}S$ films grown on glass substrate varying the stoichiometries of precursors (**2**) and (**5**). The diffraction peak of the hexagonal (002) plane shifts toward a lower angle with an increased concentration of cadmium precursors. Hence, the lattice expands on (002) as the bulkier cadmium substitutes for zinc.

The (002) spacing plane calculated from the films deposited varying the ratio of precursors (**1**) and (**4**) are 3.1882 Å, x = 0.50 and 3.3482 Å, x = 0.75. The lattice distances (d) for (**2**) and (**5**) are 3.2507 Å, x = 0.25; 3.3406 Å, x = 0.50; and 3.3605 Å, x = 0.75 (Figure11). The calculated lattice distances (d) for precursors (**3**) and (**6**) are 3.1349 Å, x = 0.25; 3.1565 Å, x = 0.50; and 3.2583 Å, x = 0.75.

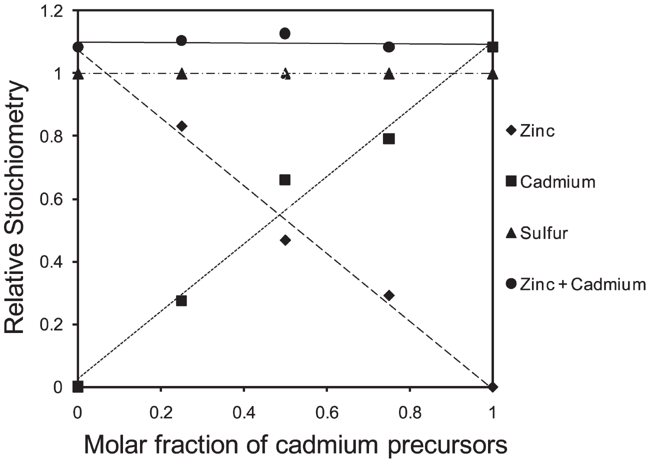

Figure 13. Graph showing molar fraction cadmium precursors vs relative stoichiometry zinc, cadmium, and sulfur from films deposited using precursors (**1**) and (**4**) analyzed by EDX.

The shift in diffraction angle clearly indicates the formation of a $Zn_xCd_{1-x}S$ solid state solution. Figure 12 shows the increase in lattice distances proportional to the increasing concentration of cadmium precursors.

Morphological Studies. The films of $Zn_xCd_{1-x}S$ were deposited by varying the ratio of zinc to cadmium were imaged by SEM (Supporting Information). Granular spherical crystallites were deposited using precursors (**1**) and (**4**) with the a diameter size of 235 ± 30 nm at 0.25, 255 ± 20 nm at 0.50, and 280 ± 25 nm at 0.75 molar fraction of (**4**) obtained. Granular cluster-like morphology of films were deposited using precursors (**2**) and (**5**) with diameter size of 550 ± 30 nm at 0.25, 570 ± 25 nm, and 300 ± 25 nm at 0.5 and 0.75 molar fraction of (**5**). SEM

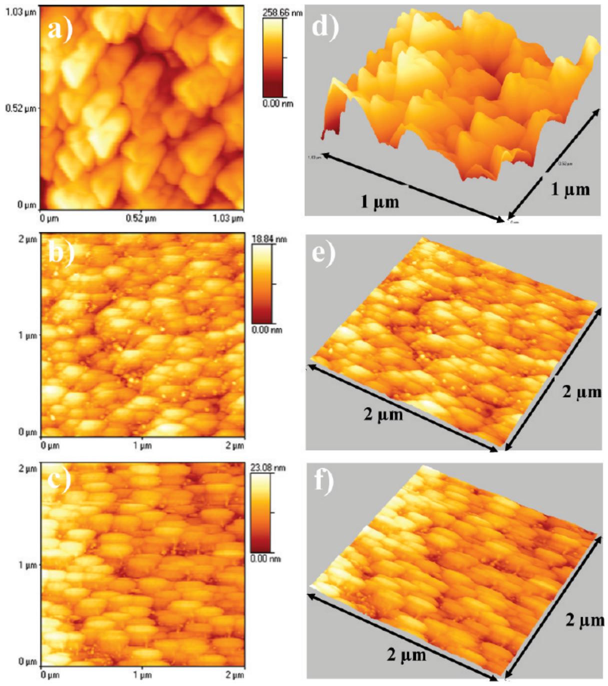

Figure 14. AFM images of $Zn_xCd_{1-x}S$ films deposited at 400 °C. (a) and (d): 2-D and 3-D images of films from complexes (**1**) and (**4**). (b) and (e): 2-D and 3-D images of films from complexes (**2**) and (**5**). (c) and (f): 2-D and 3-D images of films from complexes (**3**) and (**6**).

image of films deposited using precursors (**3**) and (**6**) showed granular clusters of crystallites with diameter size of 700 ± 50 nm at 0.25, 575 ± 25 nm at 0.50, and 500 ± 30 nm at 0.75.

EDX analysis of the films deposited at differing ratios of precursor (x = mole fraction of Cd) enables an estimate of elemental composition. Precursors (**1**) and (**4**) gave respective percentages of Zn, Cd, and S as 39.5, 13.0, and 47.5 at $x = 0.25$; 22.0, 31.0, and 47.0 at $x = 0.50$; and 14.0, 38.0, and 48.0 at $x = 0.75$. The percent composition of films deposited using precursors (**2**) and (**5**) for Zn, Cd, and S are 24.7, 38.6, and 36.5 at $x = 0.25$; 22.5, 36.6, and 40.8 at $x = 0.50$; and 14.7, 42.6, and 42.6 at $x = 0.75$. Films deposited using precursors (**3**) and (**6**) gave percentages of Zn, Cd, and S of 20.4, 29.3, and 50.2 at $x = 0.25$; 26.6, 26.1, and 47.2 at $x = 0.50$; and 13.7, 34.6, and 51.6 at $x = 0.75$. These results are illustrated in Figure 13. The EDX results confirm that the variation in zinc and cadmium compositions are almost linear for precursor pair (**1**) and (**4**), which is consistent with results with obtained from powder XRD results.

AFM analysis shows the presence of uniform and crack-free surfaces characterized by well-interconnected globular crystallites as in Figure 14. The average roughness was 35−45 nm , appreciably higher than ZnS and CdS films deposited at 400 °C using precursors (**1**) and (**4**). AFM images show films deposited using precursors (**2**) and (**5**) consist of cluster-like crystallites with an average roughness of 50−72 nm. Similarly, the films deposited from precursors (**3**) and (**6**) are composed of crack-free globular crystallites with an average roughness of 45−63 nm.

CONCLUSION

The zinc or cadmium complexes of 1,1,5,5-tetraalkyl-2-4-dithiobiurets $[M(N(SCNR_2)_2)_2]$ [M = Zn, R = methy (**1**), ethyl (**2**) and M = Cd, R = methyl (**4**), ethyl (**5**)] and 1,1,5,5-tetraalkyl-2-thiobiurets $[M(SON(CNR_2)_2)_2]$ [M = Zn, R = isopropyl (**3**) and M = Cd, R = isopropyl (**6**)] have been synthesized. The single crystal X-ray structures of complexes (**2**), (**3**), (**4**), and (**5**) revealed Zn(II) and Cd(II) ions in tetrahedral geometries. AACVD from complexes (**1**) and (**3**) gave cubic ZnS films with small rods and granular crystallites at 300 and 350 °C, whereas at 400 and 450 °C hexagonal ZnS with granular crystallites were deposited. Complex (**2**) gave hexagonal ZnS films with granular crystallites at all deposition temperatures. Similarly, cadmium complexes (**4**), (**5**), and (**6**) gave hexagonal CdS granular films at all deposition temperatures. $Zn_xCd_{1-x}S$ films were deposited by varying the molar ratio of precursors (**1**):(**4**), (**2**):(**5**), and (**3**):(**6**) at 400 °C. The optical band gaps (UV−vis), powder X-ray diffraction, and energy dispersive X-ray spectroscopy confirmed the formation of a $Zn_xCd_{1-x}S$ solid solution.

ASSOCIATED CONTENT

Ⓢ Supporting Information. Crystallographic information files (CIF) for compounds **2, 3, 4**, and **5** as electronic copies. This material is available free of charge via the Internet at http://pubs.acs.org.

AUTHOR INFORMATION

Corresponding Author

*E-mail: paul.obrien@manchester.ac.uk.

ACKNOWLEDGMENT

K.R. is grateful to ORS and The University of Manchester for financial support. The authors also thank EPSRC, U.K., for the grants to P.O.B. that have made this research possible.

REFERENCES

(1) Brafman, O.; Alexander, E.; Steinberger, I. T. *Acta Crystallogr.* **1967**, *22*, 347.

(2) Mardix, S.; Brafman, O.; Steinberger, I. T. *Acta Crystallogr.* **1967**, *22*, 805.

(3) Ramsdell, L. S. *Am. Mineral.* **1947**, *32*, 64.

(4) Pike, R. D.; Cui, H.; Kershaw, R.; Dwight, K.; Wold, A.; Blanton, T. N.; Wernberg, A. A.; Gysling, H. J. *Thin Solid Films* **1993**, *224*, 221.

(5) Shay, J. L.; Spicer, W. E.; Herman, F. *Phys. Rev. Lett.* **1967**, *18*, 649.

(6) Bube, R. H. *Physics and Chemistry of II−VI Semiconductors*; Interscience, Wiley: North Holland, Amsterdam, 1967.

(7) Ray, B. *Physics and Chemistry of II−VI Compounds*; Pergamon Press: Oxford, 1969.

(8) Boyle, D. S.; O'Brien, P.; Otway, D. J.; Robbe, O. *J. Mater. Chem.* **1999**, *9*, 725.

(9) Bayer, A.; Boyle., D. S.; Heinrich, M. R.; O'Brien, P.; Otway, D. J.; Robbe, O. *Green. Chem.* **2000**, 79.

(10) Mariano, A. N.; Warekois, E. P. *Science* **1963**, *142*, 672.

(11) Rooymans, C. J. M. *Phys. Rev. Lett.* **1963**, *4*, 186.

(12) Kabalkina, S. S.; Troitskaya, Z. V. *Dokl. Akad. Nauk SSSR* **1963**, *151*, 1068.

(13) Teodorescu, G.; Jitanu, G.; Ciomistan, D. *Rev. Romm. Phys.* **1972**, *17*, 71.

(14) Fujite, M. *J. Phys. Soc. Jpn.* **1965**, *20*, 109.

(15) Fowler, A. B. *J. Phys. Chem. Solids* **1961**, *22*, 181.

(16) Nicolau, Y. F.; Dupuy, M.; Brunel, M. *J. Electrochem. Soc.* **1990**, *137*, 2915.

(17) Nyman, M.; Jenkins, K.; Hampden-smith, M. J.; Kodas, T. T.; Duesler, E. N. *Chem, Mater.* **1998**, *10*, 914 and references therein.

(18) Tsuji, M.; Aramoto, T.; Ohyama, H.; Hibino, T.; Omura, K. *Jpn. J. Appl. Phys.* **2002**, *39*, 3902.

(19) Wei, M.; Choi, K. L. *Chem. Vap. Deposition* **2002**, *8*, 15.

(20) Ortiz, A.; Alonso, J. C.; Pankov, V. *J. Mater. Sci. Mater. Electron.* **1999**, *10*, 503.

(21) Kushida, T.; Kurita, A. *J. Lumen.* **2000**, *87*−*89*, 466.

(22) Kryshtab, T. G.; Khomchenko, V. S.; Papusha, V. P.; Mazin, M. O.; Tzyrkunov, Y. A. *Thin Solid Films* **2002**, *403*−*404*, 76.

(23) Salem, A. M. *Appl. Phys. A: Mater. Sci. Process.* **2002**, *74*, 205–211.

(24) Singh, V. P.; Singh, S. *Czech. J. Phys. B.* **1976**, *26*, 1161.

(25) Yamaguchi, T.; Matsufusa, J.; Yoshida, A. *Jpn. J. Appl.Phys.* **1992**, *31*, L703.

(26) Walter, T.; Ruckh, M.; Velthaus, K. O.; Schock, H. W. Switzerland, 1992, p 124.

(27) Feigelson, R. S; N'Diage, A.; Yin, S. Y.; Bube, R. H. *J. Appl. Phys.* **1977**, *48*, 3162.

(28) Banerjee, A.; Nath, P.; Vankar, V. D.; Chopra, K. L. *Phys. Status Solidi A* **1978**, *46*, 723.

(29) Boyle, D. S.; Robbe, O.; Halliday, D. P.; Heinrich, M. R.; Bayer, A.; O'Brien, P.; Otway, D. J.; Potter, M. D. G. *J. Mater. Chem.* **2000**, *10*, 2439.

(30) Reddy, K. T. R.; Reddy, P. J. *J. Phys. D* **1992**, *25*, 1345.

(31) Basol, B. M. *J. Appl. Phys.* **1984**, *55*, 601.

(32) Jun, Y. K.; Im, H. B. *J. Electrochem. Soc.: Electrochem, Sci. Technol.* **1988**, *135*, 1658.

(33) Kim, H. S.; Im, H. B. *Thin Solid Films* **1992**, *214*, 207.

(34) Yamaguchi, T.; Yamamoto, Y.; Taniska, T.; Yoshida, H. *Thin Solid Films* **1999**, *516*, 343.

(35) Oladeji, I. O.; Chow, L.; Ferikides, C. S.; Viswanathan, V.; Zhao, Z. *Sol. Energy Mater. Sol. Cells* **2000**, *61*, 203.

(36) Wang, Z.; Griffin, P. B.; McVittie, J.; Wong, S.; McIntyre, P. C.; Nishi, Y. *IEEE Electron Device Lett.* **2007**, *28*, 14.

(37) Mandal, S. K.; Chaudhuri, S.; Pal, A. K *Thin Solid Films* **1999**, *350*, 209.

(38) Tsai, C. T.; Chuu, D. S.; Chen, G. L.; Yang, S. L. *J. Appl. Phys.* **1996**, *79*, 9105.

(39) Mclaughin, M.; Sakeek, H.; Maguire, P. *Appl. Phys. Lett.* **1993**, *63*, 1865.

(40) Ullrich, B.; Sakai, H.; Segawa, Y. *Thin Solid Films* **2001**, *385*, 220.

(41) Afifi, H. H.; Mahmoud, S. A.; Ashour, A. *Thin Solid Films* **1995**, *263*, 248.

(42) Baykul, M. C.; Balcioglu, A. *Microelectron. Eng.* **2000**, *51*−*52*, 703.

(43) Nèmec, P.; Nèmec, I.; Nahalkova, Y.; Trojaner, F.; Maly, P. *Thin Solid Films* **2002**, *403* − *404*, 9.

(44) Wei, M.; Choi, K. L. *Chem. Vap. Deposition* **2002**, *8*, 15.

(45) Su, B.; Wei, M.; Choy, K. L. *Mater. Lett.* **2001**, *47*, 83.

(46) Tang, W.; Cameron, D. C. *Thin Solid Films* **1996**, *280*, 221.

(47) Gorer, S.; Hodes, G.; Sorek, Y.; Reisfeld, R. *Mater. Lett.* **1997**, *31*, 209.

(48) Kuroyanagi, A. *Thin Solid Films.* **1994**, *249*, 91.

(49) Barreca, D.; Gasparotto, A.; Maragno, C.; Tondello, E.; Sada, C. *Chem. Vap. Deposition.* **2004**, *10*, 229.

(50) Ramasamy, K.; Malik, M. A.; O'Brien, P.; Raftery, J. *Dalton Trans.* **2009**, 2196.

(51) Ajayi, O. B.; Osuntola, O. K.; Ojo, I. A.; Jeynes, C. *Thin Solid Films* **1994**, *248*, 57.

(52) Hursthouse, M. B.; Azad Malik, M.; Motevalli, M.; O'Brien, P. *Organometallics* **1991**, *10*, 730.

(53) Frigo, D. M.; Khan, O. F. Z.; O'Brien, P. *J. Cryst. Growth* **1989**, *96*, 989.

(54) Byrom, C.; Malik, M. A.; O'Brien, P.; White, A. J. P. *Polyhedron* **2000**, *19*, 211.

(55) Nyman, M.; Hampten-Smith, M. J.; Duesler, E. *Chem. Vap. Deposition* **1996**, *2*, 171.

(56) Ramasamy, K.; Malik, M. A.; O'Brien, P.; Raftery, J. *Mater. Res. Soc. Symp. Proc.* **2009**, *1145*, MM 04–40.

(57) Ramasamy, K.; Malik, M. A.; O'Brien, P.; Raftery, J. *Dalton Trans.* **2010**, *39*, 1460.

(58) Ramasamy, K.; Malik, M. A.; Helliwell, M.; Tuna, F.; O'Brien, P. *Inorg. Chem.* **2010**, *49*, 8495.

(59) Ramasamy, K.; Malik, M. A.; Raftery, J.; Tuna, F.; O'Brien, P. *Chem. Mater.* **2010**, *22*, 4919.

(60) Ramasamy, K.; Malik, M. A.; Helliwell, M.; O'Brien, P. *Chem. Mater.* **2010**, *22*, 6328.

(61) Ramasamy, K.; Weerakanya, M.; Malik, M. A.; O'Brien, P. *Philos. Trans. R. Soc., A* **2010**, *368*, 4249.

(62) Sheldrick, G. M. *SHELXS-97, SHELXL-97*; University of Göttingen: Göttingen, Germany, 1997.

(63) *SHELXTL*, version 6.12; Bruker AXS, Inc.: Madison, WI, 2001.

(64) Armstrong, K. E.; Crane, J. D.; Whittingham, M. *Inorg. Chem. Commun.* **2004**, *7*, 784.

(65) Fan, D.; Afzaal, M.; Mailk, M. A.; Nguyen, C. Q.; O'Brien, P.; Thomas, J .*Coord. Chem. Rev.* **2007**, *251*, 1878.

(66) Barreca, D.; Gasparotto, A.; Maragno, C.; Tondello, E. *J. Electrochem. Soc.* **2004**, *151*, G428.

(67) Ichimura, M.; Goto, F.; Arai, E. *J. Appl. Phys.* **1999**, *85*, 7411.

(68) Wang, Y. G.; Lau, S. P.; Lee, H. W.; Yu, S. F.; Tay, B. K.; Zhang, H. X.; Hng, H. H. *J. Appl. Phys.* **2003**, *94*, 354.

(69) Fujihara, S.; Sasaki, C.; Kimura, T. *Appl. Surf. Sci.* **2001**, *180*, 341.

(70) Lee, D. N. *Thin Solid Films* **2003**, *434*, 183.

(71) Nikolic, L. M.; Radonjic, L.; Srdic, V. V. *Ceram. Int.* **2005**, *31*, 261.

(72) Hichou, A. E.; Addou, M.; Bubendorff, J. L; Ebothe, J.; Idrissi, B. E.; Troyon, M. *Semicond. Sci. Technol.* **2004**, *19*, 230.

(73) Scott, S. D.; Barnes, H. L. *Geochim. Cosmochim. Acta* **1972**, *86*, 1275.

(74) Johnston, D. A.; Carletto, M. H.; Reddy, K. T. R.; Forbes, I.; Miles, R. W. *Thin Solid Films* **2002**, *403*, 102.

(75) Cheng, J.; Fan, D. B.; Wang, H.; Liu, B. W.; Zhang, Y. C.; Yan, H. *Semicond. Sci. Technol.* **2003**, *18*, 676.

(76) Saratale, S. D.; Sankapal, B. R.; Lux-Steiner, M.; Ennaoui, A. *Thin Solid Films* **2005**, *480*, 168.

(77) Lee, J.; Lee, S.; Cho, S.; Kim, S.; Park, I. Y.; Choi, Y. D. *Mater. Chem. Phys.* **2002**, *77*, 254.

(78) Elidrissi, B.; Addou, M.; Regragui, M.; Bougrine, A.; Akchouane, A.; Bernede, J. C. *Mater. Chem. Phys.* **2001**, *68*, 175.

(79) Chopra, K. L. *Thin Solid Phenomena*; McGraw-Hill: New York, 1969.

(80) Druz, B. L.; Dyadenko, A. I.; Evtukhov, Y. V.; Rakhlin, M. Y.; Rodionov, V. E. *Inorg. Mater.* **1990**, *26*, 24.